

Higher-order spatial photon interference versus dipole blockade effect

Arthur Rotari and Mihai A. Macovei*

Institute of Applied Physics, Moldova State University, Academiei str. 5, MD-2028 Chişinău, Moldova

(Dated: February 23, 2026)

The steady-state quantum dynamics of three dipole-dipole coupled two-level emitters, fixed at the vertices of an equilateral triangle, and interacting via the environmental thermostat is investigated. We have analytically obtained the populations of the involved three-atom cooperative states as well as of the second- and third-order spatial photon correlation functions of the light scattered by the few-qubit sample. As a consequence, we have demonstrated that this incoherently excited system spontaneously generates streams of single photons possessing sub-Poissonian photon statistics. In analogy to the dipole-dipole blockade, one may expect that at smaller inter particle distances, compared to the photon emission wavelength, the reported phenomenon has the same origin. However, we have shown that the quantum photon features are due to the interaction's nature of the few symmetrically arranged two-level emitters with the surrounding thermal reservoir. Respectively, at larger atomic intervals the effect occurs because of high-order spatial interference phenomena. Sub-wavelength interference fringes can be observed too, via measurements of spatial higher-order photon correlation functions.

I. INTRODUCTION

Generally, the light naturally emitted around us by various objects possesses classically incoherent properties. However, the applications of modern technologies, including quantum ones, may require photon flows with quantum properties. Therefore, over the years, this topic has been widely investigated while the research leading to the generation of such photons is still being of great interest. Particularly, among those studies on quantum light generation is the work on photon anti-bunching in resonance fluorescence of sodium atoms continuously excited by a dye-laser beam [1]. Squeezed light in single-atom resonance fluorescence occurs as well [2]. Furthermore, the squeezing phenomenon can be even stronger in resonance fluorescence processes if N atoms, distributed at regular positions, are involved [3].

In order to generate single-, two- or multiple-photon quantum states, which are of practical interest too, the photon blockade effect may be involved. It is based on employing various Kerr-like non-linearities [4, 5], strong qubit-cavity couplings [6–8] or coupled resonators [9, 10], for instance. On the other side, when more than a single-qubit is considered, the strong dipole-dipole interactions among closely spaced few-level emitters cause shifting of the collective energy levels, resulting in off-resonant laser excitations. This leads to the so called dipole blockade phenomenon which can be used to inhibit excitation of higher collective states [11–14].

In this context, quantum features can be obtained even when the emitters interact with incoherent light or environmental thermal electromagnetic field reservoirs. For instance, entanglement between two arbitrary qubits can be generated if they interact with a common thermal bath [15, 16], see also criteria for three-qubit entangle-

ment [17]. A collection of strongly dipole-dipole interacting two-level emitters through the surrounding thermostat, in the Dicke limit, was shown to generate photons with sub-Poissonian statistics [18]. Remarkably, though counterintuitively, thermal light induces sub-wavelength interferences [19] which is a quantum effect as well, see also Refs. [20, 21]. Enhanced directional emission of spontaneous radiation can be produced also with statistically independent incoherent sources, via the measurement of higher-order correlation functions of the emitted radiation [22], see also [23–25]. It was shown there that in a linear chain of independent two-level emitters, the superradiance and the Hanbury Brown-Twiss effect basically complement each other.

Here, we theoretically investigate the interaction of a small system consisting of three quantum emitters (e.g. real or artificial atoms having two energy levels) which is mediated by the surrounding thermal electromagnetic field reservoir. The atomic subsystem is spatially arranged to form an equilateral triangle, see Figure (1). Particularly, the focus is on the photon-scattering effects by the few-level quantum emitters which are excited incoherently by the thermostat, whereas the aim is being the quantum nature of these photons. In this context, we study the steady-state quantum dynamics of the considered sample and have obtained the atomic populations as well as the second- and the third-order spontaneously scattered photon correlation functions. The later are given as a function of detectors positions, respectively. We have found that for the employed geometrical arrangement of the atomic sample, the dipole-dipole interaction does not affect the steady-state properties of the photon scattering phenomenon. Hence, the sub-Poissonian photon statistics observed in the Dicke limit is rather due to the nature of the atoms-thermostat interaction and not because of the dipole-dipole blockade. Respectively, at larger inter atomic distances, the generated single photons stream possess quantum features too, however, in certain space directions. Further-

* mihai.macovei@ifa.usm.md

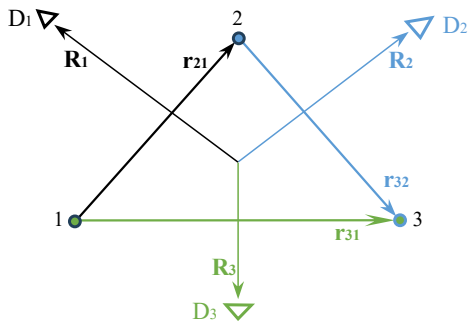


FIG. 1. Schematic picture of the considered system. Three atoms, $j \in \{1, 2, 3\}$, are arranged to form an equilateral triangle. Detectors D_k , placed at \mathbf{R}_k , $k \in \{1, 2, 3\}$, detect the spontaneously scattered photons by the atomic sample. Respectively, \mathbf{r}_{ji} are the inter atomic distance vectors and one assumes that $|\mathbf{R}_k| \gg |\mathbf{r}_{ji}|$.

more, if two detectors are placed in symmetric positions, sub-wavelength interference fringes can be observed via measurements of the spatial second-order photon-photon correlation function. It happens because of the higher-order spatial quantum interference phenomena in thermal environments.

Other relevant works have demonstrated that dipole-dipole interacting three-atom systems in external electromagnetic fields may break the dipole blockade [26] or can form three-body bound states [27], respectively. Three-qubit samples might be quite useful in context of quantum thermal transistors [28] and multifunctional quantum thermal devices [29] or in the interplay among the entanglement and non-periodic revival of spontaneous emission [30]. Three-body quantum antennas [31] or the triangular atomic mirrors [32] are additional interesting issues of the few-qubit topic.

This paper is organized as follows. In Sec. II we describe the analytical approach and the system of interest, while in Sec. III we discuss the steady-state population dynamics as well as the high-order photon correlation functions. Sec. IV presents and analyses the obtained results. The article concludes with a summary given in Sec. V.

II. THE ANALYTICAL TREATMENT

The Hamiltonian describing N two-level emitters, all having identical transition frequencies ω_0 , and mutually interacting via their environmental electromagnetic thermal reservoir is given as follows [33–37]: $H = H_0 + H_i$, where

$$H_0 = \sum_k \hbar\omega_k a_k^\dagger a_k + \sum_{j=1}^N \hbar\omega_0 S_{zj}, \quad (1)$$

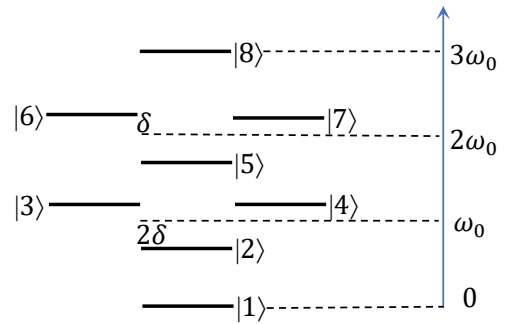


FIG. 2. The energy diagram of a spatially equidistant three-atom sample. The anti-symmetrical states $\{|6\rangle, |7\rangle\}$ and $\{|3\rangle, |4\rangle\}$ are shifted by the dipole-dipole coupling strength among the emitters, i.e. $+\delta$, whereas the symmetrical states $\{|5\rangle, |2\rangle\}$ are shifted by the doubled dipole-dipole coupling, -2δ , respectively.

and

$$H_i = i \sum_k \sum_{j=1}^N (\vec{g}_k \cdot \vec{d}_j) (a_k^\dagger S_j^- e^{-i\vec{k} \cdot \vec{r}_j} - H.c.). \quad (2)$$

Here, the first Hamiltonian, i.e. H_0 , represents the free energy of the thermal reservoir as well as the corresponding free energy of the atomic subsystem, respectively. The Hamiltonian (2) accounts for the interaction of the atomic subsystem with its surrounding thermal reservoir, where $\vec{g}_k = \sqrt{2\pi\hbar\omega_k/V} \vec{e}_p$ is the coupling strength among the few-level emitters and the thermal electromagnetic field modes, whereas \vec{e}_p is the photon polarization vector with $p \in \{1, 2\}$ and V being the quantization volume. The atomic operators defined in the usual way, i.e., $S_j^+ = |e\rangle_{jj}\langle g|$ and $S_j^- = [S_j^+]^\dagger$, obey the usual commutation relations for $\text{su}(2)$ algebra, namely, $[S_j^+, S_l^-] = 2S_{zj}\delta_{jl}$ and $[S_{zj}, S_l^\pm] = \pm S_j^\pm \delta_{jl}$, where $S_{zj} = (|e\rangle_{jj}\langle e| - |g\rangle_{jj}\langle g|)/2$ is the bare-state inversion operator of the j th qubit. Here, $|e\rangle_j$ and $|g\rangle_j$ are the excited and ground state of the emitter j , spatially localised at position \vec{r}_j , while a_k^\dagger and a_k are, respectively, the creation and the annihilation operators of the environmental electromagnetic thermal reservoir which satisfy the standard bosonic commutation relations, that is, $[a_k, a_{k'}^\dagger] = \delta_{kk'}$, and $[a_k, a_{k'}] = [a_k^\dagger, a_{k'}^\dagger] = 0$ [33–35].

Eliminating the thermal reservoir degrees of freedom, see e.g. [35–37], as usual in the Born-Markov approximations, one arrives at the following master equation describing the two-level ensemble in a thermal heat bath:

$$\begin{aligned} \frac{d}{dt} \rho(t) + i \sum_{j \neq l}^N \delta_{ij} [S_j^+ S_l^-, \rho] = \\ - \frac{\gamma}{2} \sum_{j,l=1}^N \chi_{jl} \{ (1 + \bar{n}) [S_j^+, S_l^- \rho] \\ + \bar{n} [S_j^-, S_l^+ \rho] \} + H.c.. \end{aligned} \quad (3)$$

Here,

$$\delta_{jl} = \frac{3\gamma}{4} \left\{ [\cos^2 \xi_{jl} - 1] \frac{\cos(\omega_0 r_{jl}/c)}{(\omega_0 r_{jl}/c)} + [1 - 3 \cos^2 \xi_{jl}] \left[\frac{\sin(\omega_0 r_{jl}/c)}{(\omega_0 r_{jl}/c)^2} + \frac{\cos(\omega_0 r_{jl}/c)}{(\omega_0 r_{jl}/c)^3} \right] \right\},$$

are the vacuum-induced dipole-dipole interactions among any two atoms, separated by $r_{jl} = |\vec{r}_j - \vec{r}_l|$, whereas

$$\chi_{jl} = \frac{3}{2} \left\{ [1 - \cos^2 \xi_{jl}] \frac{\sin(\omega_0 r_{jl}/c)}{(\omega_0 r_{jl}/c)} + [1 - 3 \cos^2 \xi_{jl}] \left[\frac{\cos(\omega_0 r_{jl}/c)}{(\omega_0 r_{jl}/c)^2} - \frac{\sin(\omega_0 r_{jl}/c)}{(\omega_0 r_{jl}/c)^3} \right] \right\},$$

are the corresponding incoherent couplings contributing to the collective spontaneous decay [36, 37], where ξ_{jl} are the angles between the dipole moments \vec{d} , assumed identical for all atoms and parallel, and \vec{r}_{jl} . The single emitter spontaneous decay rate is given by $\gamma = 4d^2\omega_0^3/(3\hbar c^3)$, whereas $\bar{n} = [\exp(\hbar\omega_0/k_B T) - 1]^{-1}$ is the mean thermal photon number, at frequency ω_0 and temperature T , with k_B being the Boltzmann's constant, respectively. Actually, for small inter atomic separations compared to the emission wavelength, i.e. $\omega_0 r_{jl}/c \rightarrow 0$ in the Dicke limit, one has that $\chi_{jl} \rightarrow 1$, while δ_{jl} reduces to the static dipole-dipole interaction potential, i.e. $\delta_{jl} \rightarrow 3\gamma/[8(\omega_0 r_{jl}/c)^3]$. Notice that $\chi_{jl} = \chi_{lj}$ and $\delta_{jl} = \delta_{lj}$, when $j \neq l$, and $\chi_{jj} = 1$ while δ_{jj} reduces to a frequency shift, i.e. the Lamb shift, which is incorporated in the transition frequency ω_0 .

We next focus on a three-atom sample, where each emitter is being fixed at the vertices of an equilateral triangle. Therefore, the dipole-dipole coupling strengths are equal for any atomic pair, see Figure (1). Hence, $\chi_{12} = \chi_{13} = \chi_{23} \equiv \chi$, while $\delta_{12} = \delta_{13} = \delta_{23} \equiv \delta$ and we assume that $\delta/\omega_0 \rightarrow 0$. Although $\delta/\omega_0 \rightarrow 0$, the dipole-dipole-coupling strength δ can be smaller and of the same order or larger than the single-emitter spontaneous decay rate γ , however, also $\gamma/\omega_0 \rightarrow 0$. The three-atom collective Dicke states, see e.g. [38] and Figure (2), are given then as follows:

$$\begin{aligned} |8\rangle &= |e_1 e_2 e_3\rangle, \\ |7\rangle &= (|g_1 e_2 e_3\rangle - |e_1 e_2 g_3\rangle)/\sqrt{2}, \\ |6\rangle &= (-|g_1 e_2 e_3\rangle + 2|e_1 g_2 e_3\rangle - |e_1 e_2 g_3\rangle)/\sqrt{6}, \\ |5\rangle &= (|g_1 e_2 e_3\rangle + |e_1 g_2 e_3\rangle + |e_1 e_2 g_3\rangle)/\sqrt{3}, \\ |4\rangle &= (|e_1 g_2 g_3\rangle - |g_1 g_2 e_3\rangle)/\sqrt{2}, \\ |3\rangle &= (-|e_1 g_2 g_3\rangle + 2|g_1 e_2 g_3\rangle - |g_1 g_2 e_3\rangle)/\sqrt{6}, \\ |2\rangle &= (|e_1 g_2 g_3\rangle + |g_1 e_2 g_3\rangle + |g_1 g_2 e_3\rangle)/\sqrt{3}, \\ |1\rangle &= |g_1 g_2 g_3\rangle. \end{aligned} \quad (4)$$

Taking into account that [39]:

$$\begin{aligned} S_1^+ &= (R_{41} + R_{87})/\sqrt{2} + (R_{21} - R_{64} - R_{73} \\ &\quad + R_{85})/\sqrt{3} - (R_{31} + R_{54} + R_{72} + R_{86})/\sqrt{6} \\ &\quad + (R_{53} + R_{62})/\sqrt{18} + 2(R_{52} - R_{63})/3, \end{aligned}$$

$$\begin{aligned} S_2^+ &= \sqrt{2/3}(R_{31} + R_{86}) + (R_{21} + R_{85})/\sqrt{3} \\ &\quad - \sqrt{2}(R_{62} + R_{53})/3 + 2(R_{63}/2 + R_{52})/3 \\ &\quad - R_{74}, \\ S_3^+ &= -(R_{41} + R_{87})/\sqrt{2} + (R_{21} + R_{64} + R_{73} \\ &\quad + R_{85})/\sqrt{3} + (R_{54} + R_{72} - R_{31} - R_{86})/\sqrt{6} \\ &\quad + (R_{53} + R_{62})/\sqrt{18} + 2(R_{52} - R_{63})/3, \end{aligned} \quad (5)$$

with $S_j^- = [S_j^+]^\dagger$, $\{j \in 1, 2, 3\}$, the master equation (3) takes the following form in the three-atom cooperative bases, namely,

$$\begin{aligned} \frac{d}{dt}\rho(t) &+ \frac{i}{\hbar}[H, \rho] = -\frac{\gamma}{2}(1 + \bar{n})\{3(1 + 2\chi)[R_1^+, R_1^- \rho] \\ &\quad + 2(1 - \chi)[R_2^+, R_2^- \rho] + 6(1 - \chi)[R_3^+, R_3^- \rho]\} \\ &\quad - \frac{\gamma}{2}\bar{n}\{3(1 + 2\chi)[R_1^-, R_1^+ \rho] - 2(1 - \chi) \\ &\quad \times [R_2^-, R_2^+ \rho] + 6(1 - \chi)[R_3^-, R_3^+ \rho]\} + H.c., \end{aligned} \quad (6)$$

where the three-atom collective operators are defined as $R_{\alpha\beta} = |\alpha\rangle\langle\beta|$, $\{\alpha, \beta \in 1, \dots, 8\}$, satisfying the following commutation relations: $[R_{\alpha\beta}, R_{\beta'\alpha'}] = R_{\alpha\alpha'}\delta_{\beta\beta'} - R_{\beta'\beta}\delta_{\alpha'\alpha}$. In Eq. (6), $R_1^+ = (R_{21} + R_{85})/\sqrt{3} + 2R_{52}/3 - (R_{74} + R_{63})/3$, $R_2^+ = (R_{41} + R_{87})/\sqrt{2} - (R_{73} + R_{64})/\sqrt{3} - (R_{72} + R_{54})/\sqrt{6}$, and $R_3^+ = (R_{62} + R_{53})/(3\sqrt{2}) - (R_{31} + R_{86})/\sqrt{6} + (R_{74} - R_{63})/3$, with $R_j^- = [R_j^+]^\dagger$, $\{j \in \bar{1}, \bar{2}, \bar{3}\}$, respectively. The Hamiltonian H , entering in Eq. (6), is given by $H = H_q + H_{dd}$, where

$$\begin{aligned} H_q &= \hbar\omega_0(R_{22} + R_{33} + R_{44}) \\ &\quad + 2\hbar\omega_0(R_{55} + R_{66} + R_{77}) + 3\hbar\omega_0 R_{88}, \end{aligned} \quad (7)$$

while

$$\begin{aligned} H_{dd} &= -2\hbar\delta(R_{22} + R_{55}) \\ &\quad + \hbar\delta(R_{33} + R_{44} + R_{66} + R_{77}). \end{aligned} \quad (8)$$

One can observe that in the Dicke limit, when $\chi \rightarrow 1$, the master equation (6) reduces to

$$\begin{aligned} \frac{d}{dt}\rho(t) &+ \frac{i}{\hbar}[H, \rho] = -\frac{9\gamma}{2}(1 + \bar{n})[R_1^+, R_1^- \rho] \\ &\quad - \frac{9\gamma}{2}\bar{n}[R_1^-, R_1^+ \rho] + H.c., \end{aligned} \quad (9)$$

meaning that only the symmetrical three-atom collective states are involved, namely, $|8\rangle$, $|5\rangle$, $|2\rangle$ and $|1\rangle$, see Figure (2) and Exps. (4). Indeed, there are totally $N + 1 \equiv 3 + 1 = 4$ cooperative Dicke states in this particular case. The remaining anti-symmetrical three-atom collective states, i.e., $|3\rangle$, $|4\rangle$, $|6\rangle$ and $|7\rangle$ decouple from the interaction with the environmental thermal electromagnetic field reservoir and can be then omitted, in the Dicke limit. Thus, generally, the master equation (6) involves symmetrical as well as anti-symmetrical three-atom collective states, which are shifted proportional to

the dipole-dipole coupling strength δ , respectively, see Figure (2).

In the following Section, we shall focus on the steady-state collective quantum dynamics of the three-qubit sample, arranged in an equilateral triangle configuration, where both the symmetrical as well as the anti-symmetrical cooperative states are being involved.

III. EQUATIONS OF MOTION AND PHOTON CORRELATION FUNCTIONS

Using the master equation (6), one obtains the exact system of equations of motion for the mean values of the populations in the symmetrical as well as anti-symmetrical three-atom collective states:

$$\begin{aligned}
\langle \dot{R}_{11} \rangle &= -3\gamma\bar{n}\langle R_{11} \rangle + \gamma(1+2\chi)(1+\bar{n})\langle R_{22} \rangle \\
&\quad + \gamma(1-\chi)(1+\bar{n})\langle R_x \rangle, \\
\langle \dot{R}_{22} \rangle &= \gamma\bar{n}(1+2\chi)\langle R_{11} \rangle - \gamma(1+2\chi \\
&\quad + \bar{n}(3+4\chi))\langle R_{22} \rangle + \frac{4\gamma}{3}(1+\bar{n})(1+2\chi)\langle R_{55} \rangle \\
&\quad + \frac{\gamma}{3}(1+\bar{n})(1-\chi)\langle R_y \rangle, \\
\langle \dot{R}_{55} \rangle &= \frac{4\gamma}{3}\bar{n}(1+2\chi)\langle R_{22} \rangle + \gamma(1+\bar{n})(1+2\chi)\langle R_{88} \rangle \\
&\quad - \gamma(2(1+\chi) + \bar{n}(3+4\chi))\langle R_{55} \rangle \\
&\quad + \frac{\gamma}{3}\bar{n}(1-\chi)\langle R_x \rangle, \\
\langle \dot{R}_{88} \rangle &= \gamma\bar{n}(1+2\chi)\langle R_{55} \rangle - 3\gamma(1+\bar{n})\langle R_{88} \rangle \\
&\quad + \gamma\bar{n}(1-\chi)\langle R_y \rangle, \\
\langle \dot{R}_x \rangle &= 2\gamma\bar{n}(1-\chi)\langle R_{11} \rangle + \frac{2\gamma}{3}(1+\bar{n})(1-\chi)\langle R_{55} \rangle \\
&\quad - \gamma(1-\chi + \bar{n}(3-2\chi))\langle R_x \rangle + \frac{\gamma}{3}(1+\bar{n}) \\
&\quad \times (5-2\chi)\langle R_y \rangle, \\
\langle \dot{R}_y \rangle &= \frac{2\gamma}{3}\bar{n}(1-\chi)\langle R_{22} \rangle + 2\gamma(1+\bar{n})(1-\chi)\langle R_{88} \rangle \\
&\quad + \frac{\gamma}{3}\bar{n}(5-2\chi)\langle R_x \rangle - \gamma(2-\chi \\
&\quad + \bar{n}(3-2\chi))\langle R_y \rangle, \tag{10}
\end{aligned}$$

where the overdot means differentiation with respect to time, while

$$\langle R_x \rangle = \langle R_{33} \rangle + \langle R_{44} \rangle, \quad \text{and} \quad \langle R_y \rangle = \langle R_{66} \rangle + \langle R_{77} \rangle,$$

so that

$$\sum_{i=1}^8 \langle R_{ii} \rangle = 1.$$

One can observe that the populations of the symmetrical and anti-symmetrical collective states will decouple in the Dicke limit, i.e. when $\chi = 1$. Additionally, for a symmetrical geometrical arrangement of three emitters,

as it is the case here, the populations of the symmetrical states will not depend on the dipole-dipole coupling strength δ , see Eqs. (10).

For later purposes, we write down the missing equations of motion connecting, respectively, the symmetrical and anti-symmetrical three-qubit decay channels, that is,

$$\begin{aligned}
\langle \dot{R}_{33} \rangle &= \gamma\bar{n}(1-\chi)\langle R_{11} \rangle - \gamma(1-\chi + \bar{n}(3-2\chi)) \\
&\quad \times \langle R_{33} \rangle + \frac{\gamma}{3}(1+\bar{n})(1-\chi)(\langle R_{55} \rangle + 2\langle R_{77} \rangle) \\
&\quad + \gamma(1+\bar{n})\langle R_{66} \rangle - \frac{2\gamma}{3\sqrt{2}}(1+\bar{n})(1-\chi)(\langle R_{65} \rangle \\
&\quad + \langle R_{56} \rangle), \\
\langle \dot{R}_{44} \rangle &= \gamma\bar{n}(1-\chi)\langle R_{11} \rangle - \gamma(1-\chi + \bar{n}(3-2\chi)) \\
&\quad \times \langle R_{44} \rangle + \frac{\gamma}{3}(1+\bar{n})(1-\chi)(\langle R_{55} \rangle + 2\langle R_{66} \rangle) \\
&\quad + \gamma(1+\bar{n})\langle R_{77} \rangle + \frac{2\gamma}{3\sqrt{2}}(1+\bar{n})(1-\chi)(\langle R_{65} \rangle \\
&\quad + \langle R_{56} \rangle), \\
\langle \dot{R}_{66} \rangle &= \frac{\gamma\bar{n}}{3}(1-\chi)(\langle R_{22} \rangle + 2\langle R_{44} \rangle) - \gamma(2-\chi \\
&\quad + \bar{n}(3-2\chi))\langle R_{66} \rangle + \gamma\bar{n}\langle R_{33} \rangle + \gamma(1+\bar{n}) \\
&\quad \times (1-\chi)\langle R_{88} \rangle - \frac{2\gamma\bar{n}}{3\sqrt{2}}(1-\chi)(\langle R_{32} \rangle \\
&\quad + \langle R_{23} \rangle), \\
\langle \dot{R}_{77} \rangle &= \frac{\gamma\bar{n}}{3}(1-\chi)(\langle R_{22} \rangle + 2\langle R_{33} \rangle) - \gamma(2-\chi \\
&\quad + \bar{n}(3-2\chi))\langle R_{77} \rangle + \gamma\bar{n}\langle R_{44} \rangle + \gamma(1+\bar{n}) \\
&\quad \times (1-\chi)\langle R_{88} \rangle + \frac{2\gamma\bar{n}}{3\sqrt{2}}(1-\chi)(\langle R_{32} \rangle \\
&\quad + \langle R_{23} \rangle). \tag{11}
\end{aligned}$$

The equations of motion for the mean values of the off-diagonal elements, entering in Eqs. (11), are given then as follows:

$$\begin{aligned}
\langle \dot{R}_{32} \rangle &= \left\{ 3i\delta - \frac{\gamma}{2}(2+\chi + 2\bar{n}(3+\chi)) \right\} \langle R_{32} \rangle \\
&\quad - \frac{\gamma}{2}(1+\bar{n}) \left\{ \frac{4}{3\sqrt{2}}(1-\chi)(\langle R_{66} \rangle - \langle R_{77} \rangle) \right. \\
&\quad \left. - \frac{2}{3}(1-\chi)\langle R_{56} \rangle + \frac{4}{3}(1+2\chi)\langle R_{65} \rangle \right\}, \\
\langle \dot{R}_{65} \rangle &= \left\{ 3i\delta - \frac{\gamma}{2}(4+\chi + 2\bar{n}(3+\chi)) \right\} \langle R_{65} \rangle \\
&\quad - \frac{\gamma}{2}\bar{n} \left\{ \frac{4}{3\sqrt{2}}(1-\chi)(\langle R_{33} \rangle - \langle R_{44} \rangle) \right. \\
&\quad \left. - \frac{2}{3}(1-\chi)\langle R_{23} \rangle + \frac{4}{3}(1+2\chi)\langle R_{32} \rangle \right\}, \tag{12}
\end{aligned}$$

with $\langle R_{23} \rangle = [\langle R_{32} \rangle]^\dagger$ and $\langle R_{56} \rangle = [\langle R_{65} \rangle]^\dagger$.

The steady-state solutions for the mean values of the involved atomic variables as well as the corresponding spatially scattered photon correlations functions are discussed in the next subsections, respectively.

A. The steady-state solutions of the atomic variables

Setting $\langle \dot{R}_{ij} \rangle \rightarrow 0$, $\{i, j \in 1, \dots, 8\}$, in Eqs. (10-12) one arrives at the steady-state solutions for the involved atomic variables, as long as $\chi \neq 1$, describing a small ensemble formed of three spatially equidistant placed two-level emitters interacting via their thermostat, i.e.,

$$\begin{aligned} \langle R_{11} \rangle &= \left(\frac{1 + \bar{n}}{1 + 2\bar{n}} \right)^3, \\ \langle R_{22} \rangle &= \langle R_{33} \rangle = \langle R_{44} \rangle = \frac{\bar{n}(1 + \bar{n})^2}{(1 + 2\bar{n})^3}, \\ \langle R_{55} \rangle &= \langle R_{66} \rangle = \langle R_{77} \rangle = \frac{\bar{n}^2(1 + \bar{n})}{(1 + 2\bar{n})^3}, \\ \langle R_{88} \rangle &= \left(\frac{\bar{n}}{1 + 2\bar{n}} \right)^3, \end{aligned} \quad (13)$$

while $\langle R_{32} \rangle = \langle R_{23} \rangle = 0$ and $\langle R_{65} \rangle = \langle R_{56} \rangle = 0$, respectively. Actually, the symmetrical as well as the antisymmetrical three-atom collective states are populated as long as $\chi \neq 1$. Moreover, the steady state solutions (13) do not depend on the collectivity, i.e. $\{\chi, \delta\}$, or on the single-atom spontaneous decay rate γ , regardless of the distance among the emitters. For weaker thermal baths, $\bar{n} \ll 1$, one has that $\langle R_{11} \rangle \approx 1 - 3\bar{n}$ and $\langle R_{22} \rangle = \langle R_{33} \rangle = \langle R_{44} \rangle \approx \bar{n}$, while the remained higher excited collective atomic states are inhibited, see Figure (2). Bigger environmental temperatures, i.e. when $\bar{n} \gg 1$, lead to an identical population of each cooperative three-atom state which is equal to 1/8, respectively.

However, if $\chi = 1$ then from the master equation (9), or Eqs. (10), follow the following steady-state solutions for the mean values of the populations in the symmetrical three-particle states:

$$\begin{aligned} \langle R_{11} \rangle &= \frac{(1 + \bar{n})^3}{(1 + 2\bar{n})[(1 + \bar{n})^2 + \bar{n}^2]}, \\ \langle R_{22} \rangle &= \frac{\bar{n}(1 + \bar{n})^2}{(1 + 2\bar{n})[(1 + \bar{n})^2 + \bar{n}^2]}, \\ \langle R_{55} \rangle &= \frac{\bar{n}^2(1 + \bar{n})}{(1 + 2\bar{n})[(1 + \bar{n})^2 + \bar{n}^2]}, \\ \langle R_{88} \rangle &= \frac{\bar{n}^3}{(1 + 2\bar{n})[(1 + \bar{n})^2 + \bar{n}^2]}. \end{aligned} \quad (14)$$

The anti-symmetrical three-atom cooperative states are not populated since they decouple from the interaction with the thermal environment in this particular case, i.e. when $\chi = 1$. Hence, $\langle R_{11} \rangle + \langle R_{22} \rangle + \langle R_{55} \rangle + \langle R_{88} \rangle = 1$. Again, here, for lower surrounding temperatures, that is when $\bar{n} \ll 1$, one has that $\langle R_{11} \rangle \approx 1 - \bar{n}$ and $\langle R_{22} \rangle \approx \bar{n}$, whereas the steady-state populations of higher excited collective states $|5\rangle$ and $|8\rangle$ are too small. Stronger thermal heat baths, i.e. $\bar{n} \gg 1$, lead to $\langle R_{11} \rangle = \langle R_{22} \rangle = \langle R_{55} \rangle = \langle R_{88} \rangle = 1/4$ in the steady-state.

Generalising at this phase, regardless of the values of χ , $0 \leq \chi \leq 1$, at weaker thermal baths single-excitation

collective states get populated preponderantly, whereas at stronger environmental heat reservoirs all the involved three-qubit cooperative states are equally populated, respectively. Actually, the cooperative three-qubit states are populated according to the Boltzmann distribution, see Exps. (13,14).

In the following section, we shall use the steady-state populations, given by expressions (13) and (14), in order to investigate the spatial photon correlations phenomena.

B. Spatial photon correlation functions

In the far-zone limit of experimental interest, the first- and the unnormalized second-order spatial photon correlation functions at position \vec{R} , with $R = |\vec{R}| \gg \lambda$, can be represented as follows, see e.g. [33-37, 40, 41],

$$G_1(\vec{R}; t) = \sum_{j,l=1}^N \Phi_R(\vec{r}_{jl}) \langle S_j^+(t) S_l^-(t) \rangle, \quad (15)$$

and

$$\begin{aligned} G_2(\vec{R}_1, \vec{R}_2; t) &= \sum_{j_1, l_1=1}^N \sum_{j_2, l_2=1}^N \Phi_{R_1}(\vec{r}_{j_1 l_1}) \Phi_{R_2}(\vec{r}_{j_2 l_2}) \\ &\times \langle S_{j_1}^+(t) S_{j_2}^+(t) S_{l_2}^-(t) S_{l_1}^-(t) \rangle, \end{aligned} \quad (16)$$

whereas the unnormalized third-order spatial photon correlation function is given by the next expression [36, 40, 41], respectively,

$$\begin{aligned} G_3(\vec{R}_1, \vec{R}_2, \vec{R}_3; t) &= \sum_{j_1, l_1=1}^N \sum_{j_2, l_2=1}^N \sum_{j_3, l_3=1}^N \Phi_{R_1}(\vec{r}_{j_1 l_1}) \Phi_{R_2}(\vec{r}_{j_2 l_2}) \Phi_{R_3}(\vec{r}_{j_3 l_3}) \\ &\times \langle S_{j_1}^+(t) S_{j_2}^+(t) S_{j_3}^+(t) S_{l_3}^-(t) S_{l_2}^-(t) S_{l_1}^-(t) \rangle. \end{aligned} \quad (17)$$

Here, $\Phi_R(\vec{r}_{jl}) = \Phi_R e^{i\frac{\omega_0}{c}(|\vec{R}-\vec{r}_l| - |\vec{R}-\vec{r}_j|)}$, while $\Phi_R = d^2 \omega_0^4 (1 - \cos^2 \eta) / (2c^4 |\vec{R} - \vec{r}_j| |\vec{R} - \vec{r}_l|)$ with η being the angle between the direction of vector \vec{R} and the dipole \vec{d} .

Based on Exps. (15-17), the normalized second-order photon-photon spatial correlation function is defined as [36, 40, 41]:

$$g^{(2)}(\vec{R}_1, \vec{R}_2; t) = \frac{G_2(\vec{R}_1, \vec{R}_2; t)}{G_1(\vec{R}_1; t) G_1(\vec{R}_2; t)}, \quad (18)$$

whereas the normalised third-order spatial photon correlation function is given by the following expression [36, 40, 41]:

$$g^{(3)}(\vec{R}_1, \vec{R}_2, \vec{R}_3; t) = \frac{G_3(\vec{R}_1, \vec{R}_2, \vec{R}_3; t)}{G_1(\vec{R}_1; t) G_1(\vec{R}_2; t) G_1(\vec{R}_3; t)}. \quad (19)$$

Actually, we are interested in the steady state behaviours of the higher-order photon correlation functions, that is, of $g^{(2)}(0) = \lim_{t \rightarrow \infty} g^{(2)}(\vec{R}_1, \vec{R}_2; t)$ and $g^{(3)}(0) = \lim_{t \rightarrow \infty} g^{(3)}(\vec{R}_1, \vec{R}_2, \vec{R}_3; t)$.

Now, using consecutively the relations (5), which give the transformations from the single-atom operators to collective ones, and the steady-state solutions (13), one arrives at the following steady-state expressions for the spatial photon correlation functions when $N = 3$, namely,

$$G_1(\vec{R})/\Phi_R = \frac{3\bar{n}}{1 + 2\bar{n}}, \quad (20)$$

while

$$\begin{aligned} G_2(\vec{R}_1, \vec{R}_2)/\kappa_2 &= 3 + \cos\left[\frac{\omega_0 r_{21}}{c}(\cos\theta_{R_2}^{(1)} - \cos\theta_{R_1}^{(1)})\right] \\ &+ \cos\left[\frac{\omega_0 r_{31}}{c}(\cos\theta_{R_2}^{(2)} - \cos\theta_{R_1}^{(2)})\right] \\ &+ \cos\left[\frac{\omega_0 r_{32}}{c}(\cos\theta_{R_2}^{(3)} - \cos\theta_{R_1}^{(3)})\right], \quad (21) \end{aligned}$$

where $\kappa_2 = 2\Phi_{R_1}\Phi_{R_2}(\bar{n}/[1 + 2\bar{n}])^2$ with $\Phi_{R_\xi} \propto R_\xi^{-2}$ and $\xi \in \{1, 2\}$. Also, $\theta_{R_\xi}^{(\zeta)}$, $\zeta \in \{1, 2, 3\}$, are the angles between the inter particle vectors \vec{r}_{jl} , with $r_{jl} = |\vec{r}_{jl}| \equiv |\vec{r}_j - \vec{r}_l|$ and $\{j, l\} \in \{1, 2, 3\}$, and the detectors position vectors \vec{R}_ξ , $\xi \in \{1, 2\}$, respectively. While obtaining the Exps. (20,21) we have also used that the steady-state mean values of all involved off-diagonal elements are zero as well as the corresponding second-order correlators, except for $\langle S_1^+ S_1^- S_2^+ S_2^- \rangle = \langle S_1^+ S_1^- S_3^+ S_3^- \rangle = \langle S_2^+ S_2^- S_3^+ S_3^- \rangle \equiv (\bar{n}/[1 + 2\bar{n}])^2$. Notice that the first-order photon correlation function, i.e. $G_1(\vec{R})$ or the photon scattered intensity, is an isotropic function of \vec{R} and scales inversely proportional to the squared distance from the emitters to the detector. This is not the case anymore for higher-order photon correlation functions.

Correspondingly, the steady-state third-order spatial photon correlation function for the light scattered by thermally driven three-atom sample is,

$$\begin{aligned} G_3(\vec{R}_1, \vec{R}_2, \vec{R}_3)/\kappa_3 &= 3 + G_3(r_{21}) + G_3(r_{31}) + G_3(r_{32}) \\ &+ \sum_{i=1}^3 G_3^{(i)}. \quad (22) \end{aligned}$$

Here $\kappa_3 = 2\Phi_{R_1}\Phi_{R_2}\Phi_{R_3}(\bar{n}/[1 + 2\bar{n}])^3$, while

$$\begin{aligned} G_3(r_{21}) &= \cos\left[\frac{\omega_0 r_{21}}{c}(\cos\theta_{R_2}^{(1)} - \cos\theta_{R_1}^{(1)})\right] \\ &+ \cos\left[\frac{\omega_0 r_{21}}{c}(\cos\theta_{R_3}^{(1)} - \cos\theta_{R_1}^{(1)})\right] \\ &+ \cos\left[\frac{\omega_0 r_{21}}{c}(\cos\theta_{R_3}^{(1)} - \cos\theta_{R_2}^{(1)})\right], \\ G_3(r_{31}) &= \cos\left[\frac{\omega_0 r_{31}}{c}(\cos\theta_{R_2}^{(2)} - \cos\theta_{R_1}^{(2)})\right] \\ &+ \cos\left[\frac{\omega_0 r_{31}}{c}(\cos\theta_{R_3}^{(2)} - \cos\theta_{R_1}^{(2)})\right] \\ &+ \cos\left[\frac{\omega_0 r_{31}}{c}(\cos\theta_{R_3}^{(2)} - \cos\theta_{R_2}^{(2)})\right], \end{aligned}$$

and

$$\begin{aligned} G_3(r_{32}) &= \cos\left[\frac{\omega_0 r_{32}}{c}(\cos\theta_{R_2}^{(3)} - \cos\theta_{R_1}^{(3)})\right] \\ &+ \cos\left[\frac{\omega_0 r_{32}}{c}(\cos\theta_{R_3}^{(3)} - \cos\theta_{R_1}^{(3)})\right] \\ &+ \cos\left[\frac{\omega_0 r_{32}}{c}(\cos\theta_{R_3}^{(3)} - \cos\theta_{R_2}^{(3)})\right], \end{aligned}$$

respectively, whereas,

$$\begin{aligned} G_3^{(1)} &= \cos\left[\frac{\omega_0}{c}(r_{21}\cos\theta_{R_1}^{(1)} + r_{32}\cos\theta_{R_3}^{(3)} - r_{31}\cos\theta_{R_2}^{(2)})\right] \\ &+ \cos\left[\frac{\omega_0}{c}(r_{21}\cos\theta_{R_1}^{(1)} + r_{32}\cos\theta_{R_2}^{(3)} - r_{31}\cos\theta_{R_3}^{(2)})\right], \end{aligned}$$

$$\begin{aligned} G_3^{(2)} &= \cos\left[\frac{\omega_0}{c}(r_{21}\cos\theta_{R_2}^{(1)} + r_{32}\cos\theta_{R_3}^{(3)} - r_{31}\cos\theta_{R_1}^{(2)})\right] \\ &+ \cos\left[\frac{\omega_0}{c}(r_{21}\cos\theta_{R_2}^{(1)} + r_{32}\cos\theta_{R_1}^{(3)} - r_{31}\cos\theta_{R_3}^{(2)})\right], \end{aligned}$$

and

$$\begin{aligned} G_3^{(3)} &= \cos\left[\frac{\omega_0}{c}(r_{21}\cos\theta_{R_3}^{(1)} + r_{32}\cos\theta_{R_2}^{(3)} - r_{31}\cos\theta_{R_1}^{(2)})\right] \\ &+ \cos\left[\frac{\omega_0}{c}(r_{21}\cos\theta_{R_3}^{(1)} + r_{32}\cos\theta_{R_1}^{(3)} - r_{31}\cos\theta_{R_2}^{(2)})\right], \end{aligned}$$

where we have used that the only non-zero three-particle correlator is $\langle S_1^+ S_2^+ S_3^+ S_3^- S_2^- S_1^- \rangle \equiv \langle R_{88} \rangle$. Also, here, one has that $r_{21} = r_{31} = r_{32} \equiv r$, with $R \gg r$.

In the following section, we shall describe the spatial interference effects of the photons scattered by the considered three-atom sample, mutually interacting via their common thermostat. Notice that, $g^{(2)}(0) < 1$ characterizes sub-Poissonian, $g^{(2)}(0) > 1$ super-Poissonian, and $g^{(2)}(0) = 1$ Poissonian photon statistics. Furthermore, the condition $g^{(3)}(0) < g^{(2)}(0) < 1$ means that the scattered photon beam consists of non-classical single photons.

IV. RESULTS AND DISCUSSION

We proceed in the following to describe the spatial interference features based on the second- and third-order photon correlation functions, respectively. This is achieved via photon detection of the spontaneously scattered electromagnetic field by the considered three-atom sample, arranged in an equilateral triangle geometrical configuration, see Figure (1). In this respect, from Exps. (20,21) and Exp. (18) immediately follows the normalised second-order spatial photon correlation function, namely,

$$\begin{aligned} g^{(2)}(0) &= \frac{2}{9} \left\{ 3 + \cos\left[\frac{\omega_0 r_{21}}{c}(\cos\theta_{R_2}^{(1)} - \cos\theta_{R_1}^{(1)})\right] \right. \\ &+ \cos\left[\frac{\omega_0 r_{31}}{c}(\cos\theta_{R_2}^{(2)} - \cos\theta_{R_1}^{(2)})\right] \\ &\left. + \cos\left[\frac{\omega_0 r_{32}}{c}(\cos\theta_{R_2}^{(3)} - \cos\theta_{R_1}^{(3)})\right] \right\}. \quad (23) \end{aligned}$$

One can easily observe that for a two-photon detector one always has that $g^{(2)}(0) = 4/3$. The same result persists if the two detectors are oppositely placed along a line, normal to the atomic plane, which passes through the triangle's centre. If, for instance, the two detectors, $\{D_1, D_2\}$, are arranged as depicted in Figure (1), while the third one, i.e. D_3 , is being omitted then the spatial second-order photon-photon correlation function becomes

$$g^{(2)}(0) = \frac{2}{9} \{3 + \cos[\sqrt{3}\omega_0 r/c] + 2 \cos[\sqrt{3}\omega_0 r/2c]\}, \quad (24)$$

which follows from Exp. (23). If $\sqrt{3}\omega_0 r/(2c) = (\pi/2)m$, $m \in \{1, 2, 3, \dots\}$, then $g^{(2)}(0)$, given by Exp. (24), varies between $g^{(2)}(0) = 4/9$ and $g^{(2)}(0) = 4/3$, i.e., one has sub- to super-Poissonian photon statistics, respectively, see also the solid line in Figure (3). Similar result is obtained when the two detectors are situated in the atomic triangle's plane and oppositely fixed along the vector \vec{r}_{21} , resulting in the following expression for the spatial second-order photon correlation function, namely,

$$g^{(2)}(0) = \frac{2}{9} \{3 + \cos[2\omega_0 r/c] + 2 \cos[\omega_0 r/c]\}. \quad (25)$$

Now, if $\omega_0 r/c = (\pi/2)m$, $m \in \{1, 2, 3, \dots\}$, then $g^{(2)}(0)$ lies between $g^{(2)}(0) = 4/9$ and $g^{(2)}(0) = 4/3$, too. The first minimum of $g^{(2)}(0)$ in Figure (3), equal to $g_{min}^{(2)}(0) = 1/3$, occurs at $x/\pi = 2/3$. Thus, generally, depending on the distances among the emitters and detector positions, the scattered photon statistics possesses quantum or close to coherent photon statistics features. Furthermore, if the two detectors are placed in symmetric positions, sub-wavelength interference fringes can be observed, see e.g. Exp. (25) and the solid line in Figure (3), where one should replace x with $x \rightarrow \omega_0 r/c$.

In the same vein, from Exp. (20) and Exp. (22), one obtains the expression for the normalized third-order spatial photon correlation function, i.e.,

$$g^{(3)}(0) = \frac{2}{27} \{3 + G_3(r_{21}) + G_3(r_{31}) + G_3(r_{32}) + \sum_{i=1}^3 G_3^{(i)}\}. \quad (26)$$

Particularly, for a single three-photon detector, from Exp. (26) follows that:

$$g^{(3)}(0) = \frac{4}{9} \{2 + \cos[\frac{\omega_0}{cR}(\vec{r}_{21} + \vec{r}_{32} - \vec{r}_{31}, \vec{R})]\}. \quad (27)$$

Since in our case $\vec{r}_{21} + \vec{r}_{32} = \vec{r}_{31}$, see Figure (1), then one obtains that $g^{(3)}(0) = 4/3$. Thus, generalizing at this stage, the probabilities to detect simultaneously a two- or a three-photon event, using a single two- or three-photon detector, are equal, i.e. $g^{(2)}(0) = g^{(3)}(0) = 4/3$, while this is being an isotropic process. In the case when three

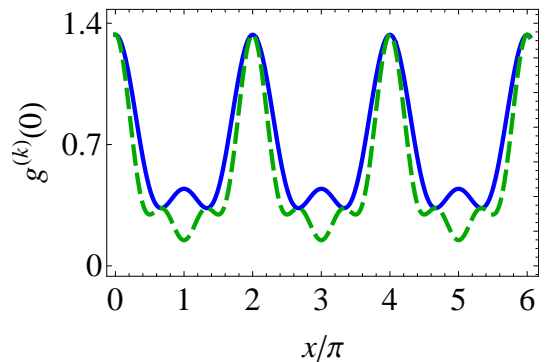


FIG. 3. The steady-state higher-order photon correlation functions $g^{(k)}(0)$ versus x/π , where $x = \sqrt{3}\omega_0 r/(2c)$, based on Exp. (24) and Exp. (28), respectively. The solid line depicts the second-order photon correlation function, i.e. $k = 2$, whereas the long-dashed curve stands for the third-order photon correlation function, where $k = 3$.

distinct photon detectors, $\{D_1, D_2, D_3\}$, are arranged as shown in Figure (1), then the spatial third-order correlation function takes the form:

$$g^{(3)}(0) = \frac{2}{27} \{7 + 3 \cos[\sqrt{3}\omega_0 r/c] + 6 \cos[\sqrt{3}\omega_0 r/2c] + 2 \cos[3\sqrt{3}\omega_0 r/2c]\}. \quad (28)$$

If, for instance, $\sqrt{3}\omega_0 r/(2c) = (\pi/2)m$, $m \in \{1, 2, 3, \dots\}$, then $g^{(3)}(0)$ ranges between $g^{(3)}(0) = 4/27$ to $g^{(3)}(0) = 4/3$, see the long-dashed curve in Figure (3). Comparing with the results for the second-order correlation function, given by Exp. (24), one observes that when $\sqrt{3}\omega_0 r/(2c) = \pi/2$, the value for $g^{(3)}(0) = 8/27$ is lower than that of $g^{(2)}(0) = 4/9$, while $g^{(2)}(0) < 1$, see also Figure (3). This indicates that streams of single photons, possessing sub-Poissonian statistics, is generating when both detectors, i.e. $\{D_1, D_2\}$, click, see Figure (1). Similar result occurs when $\sqrt{3}\omega_0 r/(2c) = 19\pi/2$, for instance. The difference here is that if $\sqrt{3}\omega_0 r/(2c) = \pi/2$, then $r/\lambda \approx 0.3$, whereas when $\sqrt{3}\omega_0 r/(2c) = 19\pi/2$, then $r/\lambda \approx 5.5$, respectively. This means that in the first case we are in the collective regime of interaction, while in the second case not. One may expect then that the single-photon emission processes, based on the condition $g^{(3)}(0) < g^{(2)}(0) < 1$, might taking place because of the dipole-dipole blockade effect occurring at smaller inter-particle distances, $r/\lambda < 1$. At larger atomic intervals, that is when $r/\lambda > 1$, the single-photon emission processes are due to spatial interference phenomena, respectively. Furthermore, if $\chi \neq 1$, the normalised spatial photon correlation functions do not explicitly depend on the thermostat's properties, although the unnormalised photon correlation functions, i.e. $\{G_1, G_2, G_3\}$, indeed depend explicitly on the mean thermal photon number \bar{n} , see Exps. (20-22).

In order to elucidate if this is indeed the case, namely, the sub-Poissonian photon statistics may occurring due

to the dipole-dipole blockade or high-order spatial interference, or something else, we shall focus next on the Dicke model for which $\chi = 1$. In this respect, the unnormalised photon correlation functions are given as: $G_1 \sim \langle S^+ S^- \rangle$, $G_2 \sim \langle S^+ S^+ S^- S^- \rangle$ and $G_3 \sim \langle S^+ S^+ S^+ S^- S^- S^- \rangle$, respectively. Correspondingly, the normalised second- and third-order photon correlation functions are defined as follows:

$$g^{(2)}(0) = \frac{\langle S^+ S^+ S^- S^- \rangle}{\langle S^+ S^- \rangle^2}, \quad (29)$$

and

$$g^{(3)}(0) = \frac{\langle S^+ S^+ S^+ S^- S^- S^- \rangle}{\langle S^+ S^- \rangle^3}, \quad (30)$$

where $S^+ = S_1^+ + S_2^+ + S_3^+$ while $S^- = [S^+]^\dagger$. Inserting,

$$\begin{aligned} S^+ &= \sqrt{3}(R_{21} + R_{85}) + 2R_{52}, \quad \text{and} \\ S^- &= \sqrt{3}(R_{12} + R_{58}) + 2R_{25}, \end{aligned}$$

which follow from (5) in the Dicke limit, into relations (29) and (30) and using the steady-state solutions (14), one arrives at the following normalised expressions for the photon correlation functions in the Dicke limit, namely,

$$g^{(2)}(0) = \frac{12(1 + 2\bar{n})^2[(1 + \bar{n})^2 + \bar{n}^2]}{[10\bar{n}^2 + 10\bar{n} + 3]^2}, \quad (31)$$

and

$$g^{(3)}(0) = \frac{36(1 + 2\bar{n})^2[(1 + \bar{n})^2 + \bar{n}^2]^2}{[10\bar{n}^2 + 10\bar{n} + 3]^3}. \quad (32)$$

Their ratio is

$$g^{(2)}(0)/g^{(3)}(0) = \frac{3 + 10\bar{n} + 10\bar{n}^2}{3[(1 + \bar{n})^2 + \bar{n}^2]}. \quad (33)$$

Respectively, the scattered intensity by the three-atom sample in the Dicke limit is

$$G_1/\Phi_R = \frac{\bar{n}(3 + 10\bar{n} + 10\bar{n}^2)}{(1 + 2\bar{n})((1 + \bar{n})^2 + \bar{n}^2)}. \quad (34)$$

Contrary to the spatially extended three-atom sample where $\chi \neq 1$, in the Dicke limit the normalised second- and third-order photon correlation functions do depend on the thermostat's properties, that is on \bar{n} , see Exps. (31,32). Particularly, if $\hbar\omega_0/(k_B T) \gg 1$, then $g^{(2)}(0) = g^{(3)}(0) = 4/3$. However, when $\hbar\omega_0/(k_B T) \ll 1$, one has that $g^{(2)}(0) = 24/25 < 1$ and $g^{(3)}(0) = 144/250$, while their ratio is $g^{(2)}(0)/g^{(3)}(0) = 10/6 > 1$. One can observe that in the Dicke limit with higher environmental temperatures, i.e. $\bar{n} \gg 1$, one has that $g^{(3)}(0) < g^{(2)}(0) < 1$ which is similar to the photon blockade effect occurring due to dipole-dipole interactions. However, the photon correlation functions do not depend on the dipole-dipole coupling strength, δ , and so does the

populations of the involved three-atom collective states. Furthermore, stronger surrounding heat reservoirs lead here to equal population of all involved three-qubit cooperative states and not preponderantly of the single-excitation cooperative state, i.e. $|2\rangle$. Hence, on the cooperative atomic transitions $|8\rangle \rightarrow |5\rangle \rightarrow |2\rangle \rightarrow |1\rangle$ streams of single photons are emitted with sub-Poissonian statistics. Larger atomic ensembles, however, will not lead to photon emissions with quantum features [42], unless δ approaches ω_0 , see Ref. [18]. Therefore, the generation of photon fluxes by considered three-atom sample, consisting of single photons which possess quantum photon statistics, occurs due to few-emitters-thermostat interaction's nature and not because of the dipole-dipole blockade phenomena.

Thus, generalizing, depending on the mutual spatial separations among the emitters, a photon flux with sub-Poissonian statistics is generated. However, the physics behind is different, namely, at shorter inter particle distances the few-atoms-thermostat interaction's nature is responsible for photon emissions with quantum properties, whereas at larger distances - the spatial interference phenomena. Furthermore, if the two detectors are placed in symmetric positions, sub-wavelength interference fringes can be observed too. In the Dicke limit, the photon emission processes are isotropic, which is not the case anymore for higher-order photon correlations in an extended three-atom sample.

Finally, there is not a smooth transition between an extended atomic sample, where $\chi \neq 1$, and the Dicke model with $\chi = 1$. The reason is that even when $\chi \rightarrow 1$, the anti-symmetrical cooperative three-atom states are populated in the steady-state according to Exps. (13). The population time of the anti-symmetrical states then is slow, proportional to $t \sim [\gamma(1 - \chi)]^{-1}$. So, at time-intervals shorter than the population time of the anti-symmetrical states, the atomic sample will behave based on the Dicke model predictions if the inter particle space intervals are short enough compared to the photon emission wavelength, λ . Note also that if $T = 0$, i.e. $\bar{n} = 0$, then $\{G_1, G_2, G_3\} = 0$ too, and the normalized second- or third-order photon correlation functions are inappropriate.

V. SUMMARY

We have investigated the spatial photon interference phenomena based on the higher order photon correlation functions, while focusing on extended or Dicke-like three-atom sample. The two-level emitters are arranged at the vertices of an equilateral triangle and dipole-dipole interact through their environmental thermostat. As a consequence, we demonstrated that the employed atomic sample spontaneously generates streams of single-photons, possessing sub-Poissonian photon statistics. Furthermore, at smaller inter particle distances the effect is due to the thermostat-few-emitters interaction's

nature, whereas at larger inter atomic distances because of high-order spatial photon interference phenomena, respectively. If the two detectors are placed in symmetric positions, sub-wavelength interference fringes can be observed as well. The photon emission process is isotropic within the Dicke limit and spatially dependent in the case

of an extended atomic model.

ACKNOWLEDGMENTS

The financial support from The Ministry of Education and Research, via grants No. 25.80012.5007.73SE and No. 011205, are gratefully acknowledged.

-
- [1] H. J. Kimble, M. Dagenais, and L. Mandel, Photon Antibunching in Resonance Fluorescence, *Phys. Rev. Lett.* **39**, 691 (1977).
- [2] D. F. Walls, and P. Zoller, Reduced Quantum Fluctuations in Resonance Fluorescence, *Phys. Rev. Lett.* **47**, 709 (1981).
- [3] W. Vogel, and D. -G. Welsch, Squeezing Pattern in Resonance Fluorescence from a Regular N-Atom System, *Phys. Rev. Lett.* **54**, 1802 (1985).
- [4] A. Imamoglu, H. Schmidt, G. Woods, and M. Deutsch, Strongly Interacting Photons in a Nonlinear Cavity, *Phys. Rev. Lett.* **79**, 1467 (1997).
- [5] R. Huang, A. Miranowicz, J.-Q. Liao, F. Nori, and H. Jing, Nonreciprocal Photon Blockade, *Phys. Rev. Lett.* **121**, 153601 (2018).
- [6] K. M. Birnbaum, A. Boca, R. Miller, A. D. Boozer, T. E. Northup, and H. J. Kimble, Photon blockade in an optical cavity with one trapped atom, *Nature* **436**, 87 (2005).
- [7] A. Faraon, I. Fushman, D. Englund, N. Stoltz, P. Petroff, and J. Vucković, Coherent generation of non-classical light on a chip via photon-induced tunnelling and blockade, *Nature Physics* **4**, 859 (2008).
- [8] Ch. Hamsen, K. N. Tolazzi, T. Wilk, and G. Rempe, Two-Photon Blockade in an Atom-Driven Cavity QED System *Phys. Rev. Lett.* **118**, 133604 (2017).
- [9] H. J. Snijders, J. A. Frey, J. Norman, H. Flayac, V. Savona, A. C. Gossard, J. E. Bowers, M. P. van Exter, D. Bouwmeester, and W. Löffler, Observation of the Unconventional Photon Blockade, *Phys. Rev. Lett.* **121**, 043601 (2018).
- [10] C. Vaneph, A. Morvan, G. Aiello, M. Féchant, M. Aprili, J. Gabelli, and J. Estève, Observation of the Unconventional Photon Blockade in the Microwave Domain, *Phys. Rev. Lett.* **121**, 043602 (2018).
- [11] M. D. Lukin, M. Fleischhauer, R. Cote, L. M. Duan, D. Jaksch, J. I. Cirac, and P. Zoller, Dipole Blockade and Quantum Information Processing in Mesoscopic Atomic Ensembles, *Phys. Rev. Lett.* **87**, 037901 (2001).
- [12] E. Urban, T. A. Johnson, T. Henage, L. Isenhower, D. D. Yavuz, T. G. Walker and M. Saffman, Observation of Rydberg blockade between two atoms, *Nature Physics* **5**, 110 (2009).
- [13] L. A. Williamson, M. O. Borgh, and J. Ruostekoski, Superatom Picture of Collective Nonclassical Light Emission and Dipole Blockade in Atom Arrays, *Phys. Rev. Lett.* **125**, 073602 (2020).
- [14] M. Chen, J. Tang, L. Tang, H. Wu, and K. Xia, Photon blockade and single-photon generation with multiple quantum emitters, *Phys. Rev. Res.* **4**, 033083 (2022).
- [15] M. C. Arnesen, S. Bose, and V. Vedral, Natural Thermal and Magnetic Entanglement in the 1D Heisenberg Model, *Phys. Rev. Lett.* **87**, 017901 (2001).
- [16] A. M. Basharov, Entanglement of atomic states upon collective radiative decay, *JETP Lett.* **75**, 123 (2002).
- [17] W. Dür, G. Vidal, and J. I. Cirac, Three qubits can be entangled in two inequivalent ways, *Phys. Rev. A* **62**, 062314 (2000).
- [18] M. A. Macovei, Dense dipole-dipole-coupled two-level systems in a thermal bath, *Phys. Rev. A* **110**, 023712 (2024).
- [19] K. Wang, and D.-Zh. Cao, Subwavelength coincidence interference with classical thermal light, *Phys. Rev. A* **70**, 041801(R) (2004).
- [20] R. S. Bennink, S. J. Bentley, and R. W. Boyd, Two-Photon Coincidence Imaging with a Classical Source, *Phys. Rev. Lett.* **89**, 113601 (2002).
- [21] G. Scarcelli, A. Valencia, and Y. Shih, Two-photon interference with thermal light, *Europhys. Lett.* **68**, 618 (2004).
- [22] S. Oettel, R. Wiegner, G. S. Agarwal, and J. von Zanthier, Directional Superradiant Emission from Statistically Independent Incoherent Nonclassical and Classical Sources, *Phys. Rev. Lett.* **113**, 263606 (2014).
- [23] S. Agne, Th. Kauten, J. Jin, E. Meyer-Scott, J. Z. Salvail, D. R. Hamel, K. J. Resch, G. Weihs, and Th. Jennewein, Observation of Genuine Three-Photon Interference, *Phys. Rev. Lett.* **118**, 153602 (2017).
- [24] A. J. Menssen, A. E. Jones, B. J. Metcalf, M. C. Tichy, S. Barz, W. S. Kolthammer, and I. A. Walmsley, Distinguishability and Many-Particle Interference, *Phys. Rev. Lett.* **118**, 153603 (2017).
- [25] M.-O. Pleinert, A. Rueda, E. Lutz, and J. von Zanthier, Testing Higher-Order Quantum Interference with Many-Particle States, *Phys. Rev. Lett.* **126**, 190401 (2021).
- [26] T. Pohl, and P. R. Berman, Breaking the Dipole Blockade: Nearly Resonant Dipole Interactions in Few-Atom Systems, *Phys. Rev. Lett.* **102**, 013004 (2009).
- [27] M. Kiffner, W. Li, and D. Jaksch, Three-Body Bound States in Dipole-Dipole Interacting Rydberg Atoms, *Phys. Rev. Lett.* **111**, 233003 (2013).
- [28] K. Joulain, J. Drevillon, Y. Ezzahri, and J. Ordonez-Miranda, Quantum Thermal Transistor, *Phys. Rev. Lett.* **116**, 200601 (2016).
- [29] B.-q. Guo, T. Liu, and Ch.-sh. Yu, Multifunctional quantum thermal device utilizing three qubits, *Phys. Rev. E* **99**, 032112 (2019).
- [30] S. Mährlein, L. Götzendörfer, K. Günthner, J. Evers, and J. von Zanthier, Birth, death, and revival of spontaneous emission in a three-atom system, *Phys. Rev. Res.* **2**, 013278 (2020).

- [31] Z.-a. Peng, G.-q. Yang, G.-m. Huang, and G.-x. Li, Directional nonclassicality of resonance fluorescence from a three-body quantum antenna via geometry-dependent frequency engineering, *Phys. Rev. A* **102**, 053715 (2020).
- [32] S. Khattak, and Q. Gulfam, Study of a transient triangular atom mirror behavior, *Phys. Lett. A* **551**, 130605 (2025).
- [33] G. S. Agarwal, *Quantum Statistical Theories of Spontaneous Emission and their Relation to Other Approaches* (Springer, Berlin, 1974).
- [34] D. F. Walls, and G. J. Milburn, *Quantum Optics* (Berlin: Springer, 1995).
- [35] M. O. Scully, and M. S. Zubairy, *Quantum Optics* (Cambridge University, Cambridge, 1997).
- [36] Z. Ficek and S. Swain, *Quantum Interference and Coherence: Theory and Experiments* (Springer, Berlin, 2005).
- [37] M. Kiffner, M. Macovei, J. Evers, and C. H. Keitel, Vacuum-induced processes in multilevel atoms, *Progress in Optics* **55**, 85 (2010).
- [38] H. S. Freedhoff, Spontaneous emission by a fully excited system of three identical atoms, *J. Phys. B: At. Mol. Phys.* **19**, 3035 (1986).
- [39] P. Bardetski, and M. A. Macovei, Dipole-dipole-interacting two-level emitters in a moderately intense laser field, *Phys. Rev. A* **110**, 043720 (2024).
- [40] R. J. Glauber, The Quantum Theory of Optical Coherence, *Phys. Rev.* **130**, 2529 (1963).
- [41] R. J. Glauber, Coherent and Incoherent States of the Radiation Field, *Phys. Rev.* **131**, 2766 (1963).
- [42] S. S. Hassan, G. P. Hildred, R. R. Puri, and R. K. Bullough, Incoherently driven Dicke model, *J. Phys. B: At. Mol. Phys.* **15**, 2635 (1982).